Research Article | Vol. 25, No. 12 | 12 Jun 2017 | OPTICS EXPRESS 13807
Optics EXPRESS

Room temperature continuous wave quantum dot cascade laser emitting at 7.2 μm

NING ZHUO,[1,3] JIN-CHUAN ZHANG,[1,3] FENG-JIAO WANG,[1,2,3] YING-HUI LIU,[1,2,3] SHEN-QIANG ZHAI,[1,3] YUE ZHAO,[1,2,3] DONG-BO WANG,[1,2,3] ZHI-WEI JIA,[1,2,3] YU-HONG ZHOU,[1,2,3] LI-JUN WANG,[1,2,3] JUN-QI LIU,[1,2,3] SHU-MAN LIU,[1,2,3] FENG-QI LIU,[1,2,3,6] ZHAN-GUO WANG,[1,3] JACOB B. KHURGIN,[4] AND GREG SUN[5,7]

[1]*Key Laboratory of Semiconductor Materials Science, Institute of Semiconductors, Chinese Academy of Sciences, P. O. Box 912, Beijing 100083, China*
[2]*College of Materials Science and Opto-Electronic Technology, University of Chinese Academy of Sciences, Beijing, China*
[3]*Beijing Key Laboratory of Low Dimensional Semiconductor Materials and Devices, P. O. Box 912, Beijing 100083, China*
[4]*Department of Electrical and Computer Engineering, Johns Hopkins University, Baltimore, MD 21218, USA*
[5]*Department of Engineering, University of Massachusetts at Boston, Boston, MA 02125, USA*
[6]*fqliu@semi.ac.cn*
[7]*Greg.Sun@umb.edu*

Abstract: We demonstrate a quantum cascade laser with active regions consisting of InAs quantum dots deposited on GaAs buffer layers that are embedded in InGaAs wells confined by InAlAs barriers. Continuous wave room temperature lasing at the wavelength of 7.2 μm has been demonstrated with the threshold current density as low as 1.89 kA/cm^2, while in pulsed operational mode lasing at temperatures as high as 110 °C had been observed. A phenomenological theory explaining the improved performance due to weak localization of states had been formulated.

OCIS codes: (140.5965) Semiconductor lasers, quantum cascade; (230.5590) Quantum-well, -wire and -dot devices; (140.3070) Infrared and far-infrared lasers.

References and links

1. J. Faist, F. Capasso, D. L. Sivco, C. Sirtori, A. L. Hutchinson, and A. Y. Cho, "Quantum cascade laser," Science **264**(5158), 553–556 (1994).
2. M. Beck, D. Hofstetter, T. Aellen, J. Faist, U. Oesterle, M. Ilegems, E. Gini, and H. Melchior, "Continuous Wave Operation of a Mid-Infrared Semiconductor Laser at Room Temperature," Science **295**(5553), 301–305 (2002).
3. J. C. Shin, M. D'Souza, Z. Liu, J. Kirch, L. J. Mawst, D. Botez, I. Vurgaftman, and J. R. Meyer, "Highly temperature insensitive, deep-well 4.8 μm emitting quantum cascade semiconductor lasers," Appl. Phys. Lett. **94**(20), 201103 (2009).
4. P. Q. Liu, A. J. Hoffman, M. D. Escarra, K. J. Franz, J. B. Khurgin, Y. Dikmelik, X. Wang, J. Fan, and C. F. Gmachl, "Highly power-efficient quantum cascade lasers," Nat. Photonics **4**(2), 95–98 (2010).
5. Y. Bai, S. Slivken, S. Kuboya, S. R. Darvish, and M. Razeghi, "Quantum cascade lasers that emit more light than heat," Nat. Photonics **4**(2), 99–102 (2010).
6. Y. Bai, N. Bandyopadhyay, S. Tsao, S. Slivken, and M. Razeghi, "Room temperature quantum cascade lasers with 27% wall plug efficiency," Appl. Phys. Lett. **98**(18), 181102 (2011).
7. K. Fujita, S. Furuta, T. Dougakiuchi, A. Sugiyama, T. Edamura, and M. Yamanishi, "Broad-gain (Δλ/λ0</~0.4), temperature-insensitive (T<0~510K) quantum cascade lasers," Opt. Express **19**(3), 2694–2701 (2011).
8. A. Lyakh, R. Maulini, A. Tsekoun, R. Go, and C. K. N. Patel, "Tapered 4.7 μm quantum cascade lasers with highly strained active region composition delivering over 4.5 watts of continuous wave optical power," Opt. Express **20**(4), 4382–4388 (2012).
9. M. Bahriz, G. Lollia, A. N. Baranov, and R. Teissier, "High temperature operation of far infrared (λ ≈20 μm) InAs/AlSb quantum cascade lasers with dielectric waveguide," Opt. Express **23**(2), 1523–1528 (2015).

#291645 https://doi.org/10.1364/OE.25.013807
Journal © 2017 Received 29 Mar 2017; revised 10 May 2017; accepted 29 May 2017; published 8 Jun 2017

Optics EXPRESS

10. A. Lyakh, M. Suttinger, R. Go, P. Figueiredo, and A. Todi, "5.6 μm quantum cascade lasers based on a two-material active region composition with a room temperature wall-plug efficiency exceeding 28%," Appl. Phys. Lett. **109**(12), 121109 (2016).
11. Y. Yao, A. J. Hoffman, and C. F. Gmachl, "Mid-infrared quantum cascade lasers," Nat. Photonics **6**(7), 432–439 (2012).
12. M. S. Vitiello, G. Scalari, B. Williams, and P. De Natale, "Quantum cascade lasers: 20 years of challenges," Opt. Express **23**(4), 5167–5182 (2015).
13. M. Razeghi, Q. Y. Lu, N. Bandyopadhyay, W. Zhou, D. Heydari, Y. Bai, and S. Slivken, "Quantum cascade lasers: from tool to product," Opt. Express **23**(7), 8462–8475 (2015).
14. N. S. Wingreen and C. A. Stafford, "Quantum-Dot Cascade Laser: Proposal for an Ultralow-Threshold Semiconductor Laser," IEEE J. Quantum Electron. **33**(7), 1170–1173 (1997).
15. C. Hsu, J. O, and P. Zory, "Intersubband quantum-box semiconductor lasers," IEEE J. Sel. Top. Quantum Electron. **6**(3), 491–503 (2000).
16. I. A. Dmitriev and R. A. Suris, "Quantum cascade lasers based on quantum dot superlattice," Phys. Status Solidi **202**(6), 987–991 (2005).
17. D. Wasserman and S. A. Lyon, "Midinfrared luminescence from InAs quantum dots in unipolar devices," Appl. Phys. Lett. **81**(15), 2848–2850 (2002).
18. S. Anders, L. Rebohle, F. F. Schrey, W. Schrenk, K. Unterrainer, and G. Strasser, "Electroluminescence of a quantum dot cascade structure," Appl. Phys. Lett. **82**(22), 3862–3864 (2003).
19. N. Ulbrich, J. Bauer, G. Scarpa, R. Boy, D. Schuh, G. Abstreiter, S. Schmult, and W. Wegscheider, "Midinfrared intraband electroluminescence from AlInAs quantum dots," Appl. Phys. Lett. **83**(8), 1530–1532 (2003).
20. D. Wasserman, T. Ribaudo, S. A. Lyon, S. K. Lyo, and E. A. Shaner, "Room temperature midinfrared electroluminescence from InAs quantum dots," Appl. Phys. Lett. **94**(6), 061101 (2009).
21. V. Liverini, A. Bismuto, L. Nevou, M. Beck, and J. Faist, "Midinfrared electroluminescence from InAs/InP quantum dashes," Appl. Phys. Lett. **97**(22), 221109 (2010).
22. V. Liverini, L. Nevou, F. Castellano, A. Bismuto, M. Beck, F. Gramm, and J. Faist, "Room-temperature transverse-electric polarized intersubband electroluminescence from InAs/AlInAs quantum dashes," Appl. Phys. Lett. **101**(26), 261113 (2012).
23. J. Brault, M. Gendry, G. Grenet, G. Hollinger, Y. Desieres, and T. Benyattou, "Role of buffer surface morphology and alloying effects on the properties of InAs nanostructures grown on InP(001)," Appl. Phys. Lett. **73**(20), 2932–2934 (1998).
24. N. Zhuo, F. Q. Liu, J. C. Zhang, L. J. Wang, J. Q. Liu, S. Q. Zhai, and Z. G. Wang, "Quantum dot cascade laser," Nanoscale Res. Lett. **9**(1), 144 (2014).
25. N. Bandyopadhyay, Y. Bai, S. Slivken, and M. Razeghi, "High power operation of $\lambda \sim 5.2$–$11\ \mu$m strain balanced quantum cascade lasers based on the same material composition," Appl. Phys. Lett. **105**(7), 071106 (2014).
26. J. C. Zhang, F. Q. Liu, S. Tan, D. Y. Yao, L. J. Wang, L. Li, J. Q. Liu, and Z. G. Wang, "High-performance uncooled distributed-feedback quantum cascade laser without lateral regrowth," Appl. Phys. Lett. **100**(11), 112105 (2012).
27. J. B. Khurgin, "Inhomogeneous origin of the interface roughness broadening of intersubband transitions," Appl. Phys. Lett. **93**(9), 091104 (2008).

1. Introduction

Over the past two decades, quantum cascade lasers (QCLs) have been constantly improved in their performance and at this point have matured into the preferred choice of coherent sources in the mid-infrared (mid-IR) spectral region for a wide range of applications [1–10]. In recent years, it appears the rate of progress in their continuous improvement has stalled and their performance indicators have plateaued that left foremost the even lower threshold currents and higher wall-plug efficiencies to be desired [11–13]. The main attribution to this lack of continued progress has long been identified as the extremely short non-radiative lifetimes commonly associated with the intersubband transitions in the quantum wells (QWs) that form the basis for QCLs. While optimization of subband design and QCL fabrication has offered some remedy to the situation, effectiveness in slowing down the fast intersubband transition rate is intrinsically limited by the strong phonon scattering between subbands with parabolic in-plane dispersions. Proposals have been put forward to drastically reduce the optical phonon scattering by removing the subband in-plane dispersion with the use of quantum dots (QDs) in place of QWs [14–16]. The fundamental idea behind this is the three-dimensional (3D) confinement of QDs that gives arise to truly discrete energy states without in-plane dispersion and therefore energy conservation required for such scattering to take place cannot be satisfied for as long as these discrete levels are not separated with energy that is equal to that

Optics EXPRESS

of an optical phonon. The proposed schemes of QD-based QCLs all required nicely patterned QDs of equal size repeated over a large number of periods which has proven to be technically impossible with even the most advanced material growth methods. Nevertheless, efforts have been made by many groups to study its feasibility [17–22]. Results published so far are mostly based on self-assembled InAs QDs and present a challenge in bringing these devices to lase and most demonstrated electroluminescence (EL). First of all, there are significant technical difficulties in growing nicely shaped InAs QD layers in InGaAs/InAlAs – the material system of choice for mid-IR QCLs, and repeating them consistently over many periods to construct the needed cascade structure. This is because the lower level of strain induced by the smaller lattice-mismatch in this material combination tends to produce quantum dashes other than dots when grown in the Stranski-Krastanov mode [21–23]. Second, QDs and their barriers are designed so that at least one of the laser states is confined inside the QDs to take advantage of their nondispersive discrete levels. The challenge presented here is the difficulty in either efficiently injecting electrons into the upper laser state or extracting them from the lower state because the 3D confined QD states have little overlap with the extended wavefunctions of the chirped superlattice transport region.

2. Laser design, fabrication and measurements

Recently, we have demonstrated a successful QD cascade laser (QDCL) with the active regions consisting of InAs QDs embedded in InGaAs QWs with GaAs and InAlAs barriers [24]. Lasing from such a device is credited with a combination of quality QDs embedded in active QWs and localization of lower laser and extraction subbands. This device with a cavity length of 3 mm has produced pulsed lasing at the wavelength of 6.15 μm up to 250 K with threshold current density of 5.36kA/cm^2 and a characteristic temperature of about 400K. Since then we have re-engineered the QDCL structure and improved the assembly of QDs and the result is a much improved device that delivered room temperature continuous-wave (CW) operation at the wavelength of 7.2 μm. The threshold current density has been reduced to 1.34 kA/cm^2 under pulsed operation at room temperature–four times of magnitude reduction, even with a shorter cavity length of 2 mm now adopted that increased mirror loss. The key to this improvement is the insertion of a thin GaAs buffer layer on top of the InAlAs barrier upon which more uniform InAs QDs are self-assembled with precise control and tunability. In this work we present the results of this latest QDCL that we have fabricated and characterized and explain the mechanism with which the QDs contribute to its improved performance.

InAs QDs grown on InP-based InGaAs/InAlAs material system tend to be quantum dashes due to the lower strain induced by the underlying buffer material. While InAs QDs can be readily grown on GaAs/AlGaAs because of their larger lattice mismatch, injection and extraction of electrons in and out of QDs prove to be problematic in this material system. In our first QDCL [24], we used a thin GaAs capping layer on top of the InAs QDs grown on tensile strained $In_{0.44}Al_{0.56}As$ to increase the lattice mismatch between InAs and its top and bottom layers, and this technique indeed produced QDs instead of dashes. While lasing was achieved, its performance was not on par with those of mid-IR QCLs based on QWs [25], primarily due to the extreme broadening of electroluminescence spectrum as a result of the size inhomogeneity of QDs compared with that of QW-based QCLs. In our new design one important modification is the insertion of a thin GaAs buffer layer on top of $In_{0.44}Al_{0.56}As$ right before the deposition of InAs to take advantage of the large lattice mismatch between InAs and GaAs and alloying effect originating from different buffer layer composition [23] compared with the previous design for the formation of self-assembled InAs QDs, and the result is the dramatically improved size uniformity of QDs. The three QD layers in each period are obtained by depositing between 2.5 to 3.5 monolayers (MLs) of InAs on the thin GaAs buffer layers (0.5-0.65 nm), all are above the critical thickness. The thicknesses of remaining QW and barriers are such that the QDCL structure is strain compensated and its

Optics EXPRESS

injection and extraction are properly lined up with the respective upper and lower laser states. Figure 1(a) illustrates the active region consisting of three layers of coupled InAs QDs in the QDCL with progressively varying QD layer thicknesses allowing for their proper energy alignment under electrical bias.

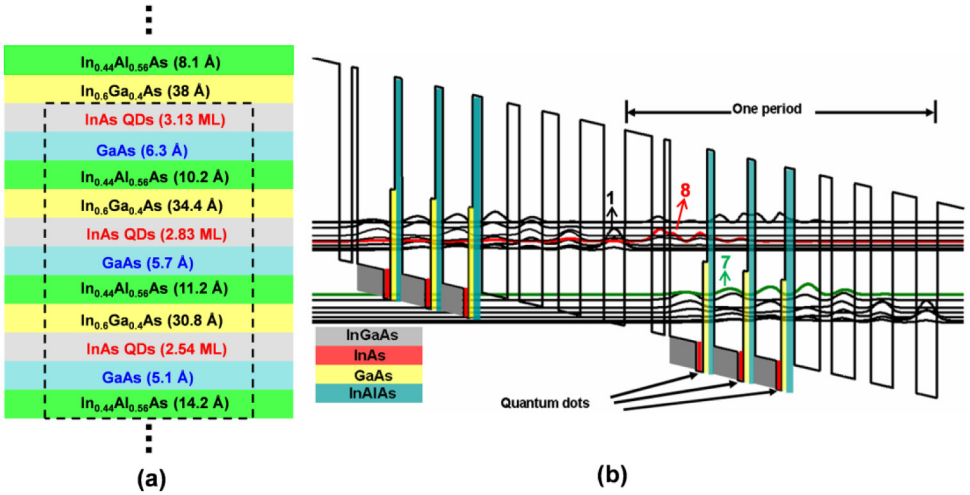

Fig. 1. (a) QDCL active region layer structure. (b) Calculated conduction band diagram and subband wavefunctions using 1D model under electric bias.

The QDCL structure was grown by molecular beam epitaxy (MBE) combined with metal-organic chemical vapor deposition (MOCVD). The epitaxial layer sequence starting from the n-doped InP substrate was as follows: 4 μm InP cladding layer (Si, 2.2e16 cm^{-3}), 0.3-μm-thick n-$In_{0.53}Ga_{0.47}As$ layer (Si, 4e16 cm^{-3}), 35 QDCL stages, 0.3-μm-thick n-$In_{0.53}Ga_{0.47}As$ layer (Si, 4e16 cm^{-3}), 3 μm upper cladding (Si, 2.6e16 cm^{-3}), and 0.75 μm cap cladding (Si, 1 e19 cm^{-3}). The QDCL operating mechanism is based on a bound-to-continuum design as shown in Fig. 1(b) in which the lasing transition takes place from the upper laser state (subband 8 in red) to the lower state (subband 7 in green). The short injectors and closely coupled injector levels, characteristics of this new design, have led to the increase of the dynamic range of the alignment voltage that can be applied to the QDCL relative to that of the former bound-to-continuum design reported in [24]. The layer sequence, with four material compositions, starting from the injection barrier is as follows (in angstroms, and InAs in ML): **40.6**/18.3/**8.1**/38/*3.13ML(InAs)*/***6.3***/**10.2**/34.4/*2.83ML(InAs)*/***5.7***/**11.2**/30.8/*2.54ML(InAs)*/***5.1***/**14.2**/36.5/**17.3**/33.5/**24.4**/31.5/**34.5**/29.4, with $In_{0.44}Al_{0.56}As$ in bold, $In_{0.6}Ga_{0.4}As$ in regular, GaAs in bold and italic, and InAs QD layer in italic, and underlined layers are doped with Si at 1.5e17 cm^{-3}. Only InP was grown by MOCVD, and the growth parameters for QDs is given in [24].

The wafer was processed into double-channel ridge waveguides using conventional photolithography and wet chemical etching. Fabrication details are identical to [26]. The average core width is 13 μm, and the waveguides were cleaved into 2-mm-long bars. The laser spectral measurements were carried out using a standard Fourier transform infrared (FTIR) spectrometer (Bruker Equinox55, Bruker Corporation, Billerica, MA, USA).The emitted optical power from laser was measured with a calibrated thermopile detector placed directly in front of the laser facet. For comparison, we have also grown and subsequently fabricated a regular QCL without the InAs QDs and the underlying GaAs buffer layers but with an increased number of cascading periods of 50.

Optics EXPRESS

3. Experimental results and analysis

The transmission electron microscopy (TEM) image in Fig. 2 shows the QDs embedded in the QDCL structure. Dark regions correspond to sites of atoms with higher atomic number (indium in this case). The image clearly reveals that there are three QD layers in a period that are nicely stacked along the growth direction, making them perpendicularly coupled and that these QDs are uncoupled horizontally with average in-plane separation of about 35 nm. The atomic force microscopy (AFM) image of the last layer of InAs QDs in the QDCL (indicated by the dashed rectangle in Fig. 1(a)) is shown as the inset in Fig. 2 with the dimension of 2.5 μm × 2.5 μm. These QDs are of elliptical shape with a short axis of ~45 nm, long axis of ~90 nm and height of ~3 nm, and slightly elongated along the [1–10] direction. The accumulation of strain around the QD sites has resulted in some interface undulation in this QDCL sample. This can potentially be improved in future with the finer control of QD sizes as well as the thicknesses and compositions of the InGaAs cladding layers as we have achieved in a single QD layer sample but not presented here.

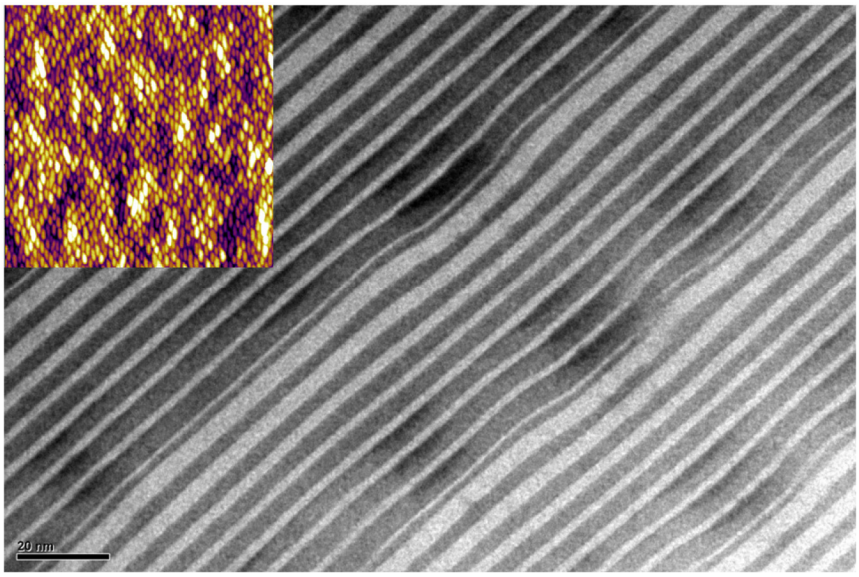

Fig. 2. TEM image of a portion of the cleaved cross section of a QDCL active region (Inset: AFM image of the last InAs QD layer in the QDCL).

Using the Bruker Equinox 55 FTIR spectrometer, we measured at room temperature the spontaneous and stimulated emission spectra from both QDCL and QCL samples as shown in Fig. 3 inset. While the small blue shift of the QDCL emission relative to that of the QCL can be accounted for by the presence of QDs, the spontaneous FWHM of QDCL is just a little bit bigger than that of QCL, indicating a high level of QD uniformity. Figure 3 shows the P-I-V curves of QDCL and QCL operating in CW mode around room temperature. At 20 °C, the CW threshold current is 490 mA for a 2-mm-long laser, corresponding to 1.89 kA/cm2, with a slope efficiency of about 1.1 W/A, from which we can deduce its internal quantum efficiency of about 55%. All these indicators are comparable with the QCL sample. Meanwhile, in pulsed mode operation at 25 °C the slope efficiency is 1.34 W/A and 1.76 W/A for QDCL and conventional QCL respectively, and considering more periods of active region in the later (50 vs. 35) this result indicates that the QDCL delivers higher efficiency owing to its better electron extraction from the lower states because of the hybridization of the QD states with the extended QW states described later.

Optics EXPRESS

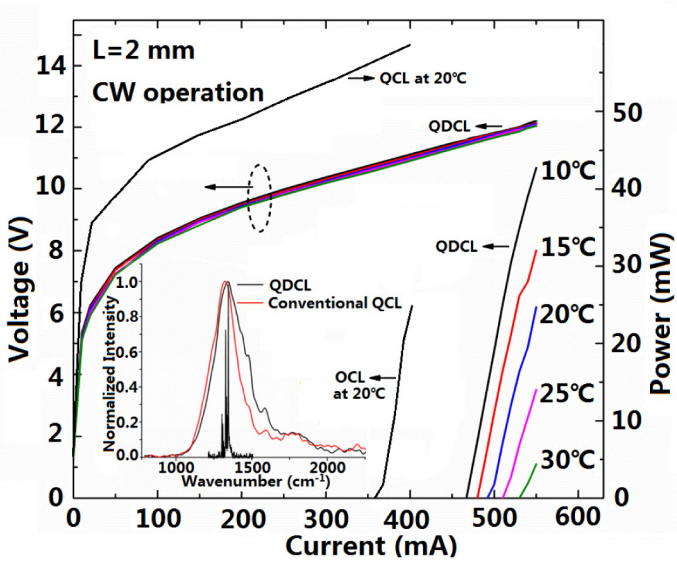

Fig. 3. P-I-V curves of QDCL and QCL operating in CW mode around room temperature. Inset: Spontaneous and stimulated emission spectra from both QDCL and QCL samples at room temperature.

Figure 4 plots the temperature dependence of the threshold current for both QDCL and QCL when driven in pulsed mode with a pulsed current source (PCX-7410). The QDCL lased slightly above 110 °C, while the QCL stopped working at 90 °C. At 283 K QDCL and QCL have the threshold density of 1.31 kA/cm2 and 0.96 kA/cm2 respectively, and considering roughly 30% reduction in the optical confinement for QDCL due to the smaller number of periods in the QDCL compared with QCL, the threshold current density of QDCL is on par with that of QCL. Within the temperature range of 283-363 K (Fig. 4(a)), T_0 of QDCL reaches 265 K, higher than 181 K of the QCL. In the lower temperature range of 80-190 K (Fig. 4(b)), T_0 of QDCL reaches a higher value of 437K, while the inset shows the thermal-tuning behavior of lasers at threshold with $\Delta\nu/\Delta T = -0.123$ cm^{-1}/K. This value is about half of that of normal FP QCLs and reveals the temperature insensitivity of spectra of QDCL, which can be attributed to relatively stronger quantum confinement effect originating from hybridization between the QD and QW states which compensates the band gap shrinking due to temperature.

Optics EXPRESS

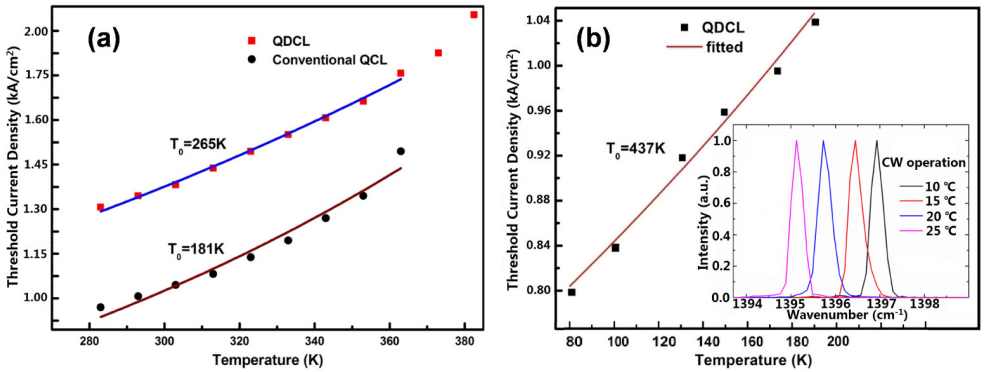

Fig. 4. Temperature dependence of the threshold current when driven in pulsed mode for (a) both QDCL and QCL within the temperature range of 283-363 K and (b) QDCL within the temperature range of 80-190 K with inset of variable temperature spectra.

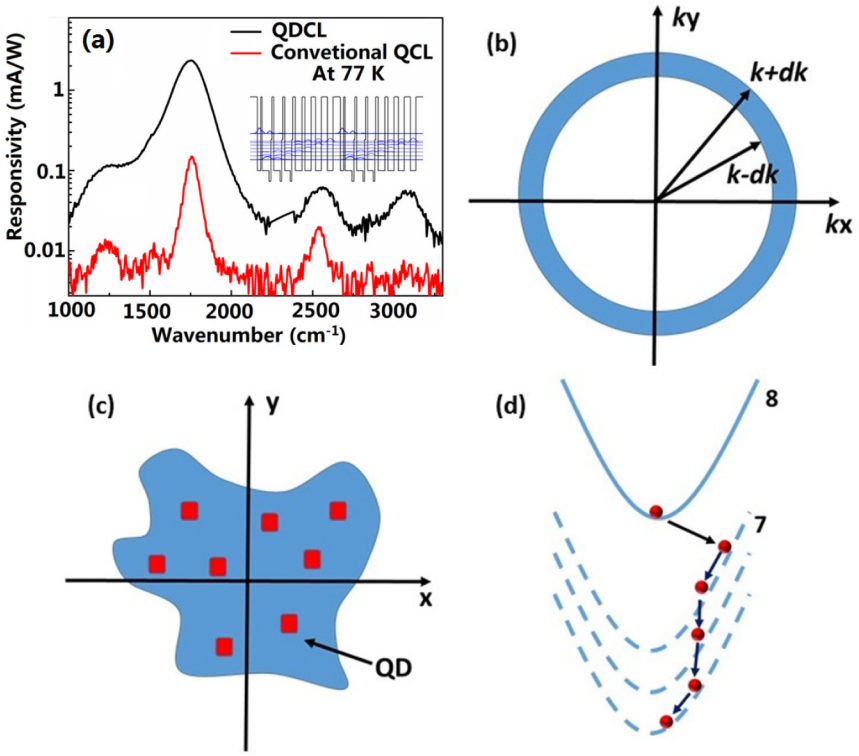

Fig. 5. (a) Responsivity of the QDCL and QCL operated as QCD at 77K under normal incident light. Illustration of (b) states in k-space within the ring of radius $\bar{k}$ and thickness $2\delta k$ that are mixed by QD scattering, (c) localized "amoeba-like" wavefunction that extends over multiple QD sites, and (d) dispersions of upper subband 8 not influenced by the QDs and lower subbands (dashed curves) that are hybridized due to QD scattering of the electrons inside QW, and electron relaxation from subband 7 into lower subbands.

The overall improvement of the lasing characteristics can be attributed to placing QDs inside the active region of the QDCL. Because the sizes and band offsets of the QDs are not sufficient to provide the strong in-plane confinement, the QD states hybridize with extended QW states and subbands are formed. The hybridization has been verified with the

Optics EXPRESS

photocurrent measurement on the same QDCL operating as a quantum cascade detector (QCD) with zero bias under the normal incidence illumination with a mid-IR source. It is well known that for optical transitions to occur between subbands in QWs, the electric field must be polarized in the direction that is perpendicular to the QW plane, eliminating the possibility that a QCD based only on QWs would be responsive to a normal incident light whose optical field is always polarized in parallel to the QW plane. This is indeed what we have observed in photocurrent measurements of the QCL sample operated as a QCD at 77K as shown in Fig. 5(a). In contrast, the QDCL sample has produced a rather appreciable photo-response that clearly indicates the hybridized nature of the states in the active region with contributions from both QW and QD characteristics. This hybridization can be thought of as being the result of QD scattering of the electrons inside a QW and the degree of hybridization reduces with the increase of electron energy simply because electrons of higher energies will be scattered less by the QDs. It is therefore not difficult to see those higher subbands consisting of injection and upper laser states should preserve mostly the characteristics of the completely delocalized QW subbands, namely the plane-wave description of the in-plane wavefunctions. In contrast to it, the lower subbands consisting of extraction and lower laser states, do get hybridized by acquiring some QD characteristics with some degree of in-plane localization. The effect of hybridization between the QD and QW states in the lower subbands is illustrated in Fig. 5(b). The role played by QDs is conceptually similar to the role played by any strong non-periodic perturbation as described in [27]. Depending on the dimension and density of the QDs the plane wave states within a certain energy range $\bar{E} \pm \delta E$, located in the k-space within the ring of radius $\bar{k} = (2m_c \bar{E} / \hbar^2)^{1/2}$ and thickness $2\delta k$, where $\delta k / \bar{k} = \delta E / 2\bar{E}$ get mixed by QD scattering and combine into new hybrid states. Each hybrid state contains wavevectors in this range of $2\delta k$ and has a localized wavefunction that extends over multiple QD sites on the scale of $\pi / \delta k$ with the probability density having an "amoeba-like" shape as depicted in Fig. 5(c). The average momenta $\bar{k}$ of different states run from 0 all the way to the maximum wavevector of the Brillouin zone, hence their kinetic energies $\bar{E}$ still follow the parabolic dispersion (dashed curves) as shown in Fig. 5(d). Obviously, transport between these states occurs mostly by hopping. Let us now consider an electron gets scattered by, say, an optical phonon, from the upper laser state in subband 8 to some high kinetic energy state in the lower subband 7. In the absence of QD scattering, this electron will relax towards the bottom of subband 7 via the ultrafast intrasubband process to populate the lower laser state. With QDs, in order for the electron to relax within the same subband, it must jump through a series of amoeba-like states. This process is hindered by the smaller overlap between different amoeba-like states in comparison to the large overlap of extended plane-wave functions in the pure QW. In addition, this slowed-down intrasubband process has to compete with electron relaxation into states of other lower subbands by jumping through their amoeba-like states as illustrated in Fig. 5(d). A positive consequence of this is the reduction of the probability of electron rolling down subband 7 and reaching its bottom relative to the probability of this electron falling down to the lower subbands and eventually into the injector. Therefore, the lower laser state 7 ends up less populated even at elevated temperatures which can be a plausible explanation for the increase in T_0 of the QDCL in comparison to that of QCL.

4. Summary

In conclusion, we have demonstrated a QDCL made of 35 cascading periods each with an active region of three layers of InAs QDs grown on GaAs buffer layers that are embedded in InGaAs QWs and InAlAs barriers. This QDCL has been operated at room temperature in CW mode at 7.2 μm. In comparison with a QCL sample without QDs but with otherwise same layer structure, the QDCL has shown better temperature performance, which we attribute to

Optics EXPRESS

the effect of hybridization between the QD and QW states and then the reduction of lower-laser-state population because of the QD scattering of electrons.

Funding

National Basic Research Program of China (Grant Nos. 2013CB632800); National Key Research and Development Program (Grant Nos. 2016YFB0402303); National Natural Science Foundation of China (NSFC) (Grant Nos. 61404131, 61435014, 61627822, 61574136, 61674144); Key projects of Chinese Academy of Sciences (Grant Nos. ZDRW-XH-2016-4, QYZDJ-SSW-JSC027); Beijing Natural Science Foundation (Grant Nos. 4162060, 4172060).

Acknowledgments

We thank Ping Liang and Ying Hu for their help in device processing.